The unstable glasma

Paul Romatschke[1] and Raju Venugopalan[2]

[1]*Fakultät für Physik, Universität Bielefeld, D-33501 Bielefeld, Germany*
[2]*Department of Physics, Bldg. 510 A, Brookhaven National Laboratory, Upton, New York-11973, USA*
(Received 25 May 2006; published 15 August 2006)

We discuss results from $3 + 1$-D numerical simulations of SU(2) Yang-Mills equations for an unstable glasma expanding into the vacuum after a high energy heavy-ion collision. We expand on our earlier work on a non-Abelian Weibel instability in such a system and study the behavior of the instability in greater detail on significantly larger lattices than previously. We establish the time scale for the onset of the instability and demonstrate that the growth rate is robust as one approaches the continuum limit. For large violations of boost invariance, non-Abelian effects cause the growth of soft modes to saturate. At late times, we observe significant creation of longitudinal pressure and a systematic trend towards isotropy. These time scales however are significantly larger than those required for early thermalization in heavy-ion collisions. We discuss additional effects in the produced glasma that may speed up thermalization.

I. INTRODUCTION

An outstanding theoretical puzzle in high energy heavy-ion collisions is to demonstrate the thermalization of the quark-gluon matter produced in these collisions. Experiments at the Relativistic Heavy Ion Collider (RHIC) at Brookhaven National Laboratory (BNL) indicate that such a thermalized state, the quark gluon plasma (QGP), has been formed in collisions of ultrarelativistic nuclear beams [1]. Understanding thermalization from first principles in quantum chromodynamics (QCD) is complicated by the interplay of several overlapping time scales. The collision itself, in the framework of the color glass condensate (CGC) effective theory [2], can be understood as the collision of coherent classical Yang-Mills fields [3,4]. The typical momenta of these fields are characterized by the scale[1] Q_s [5,6]. Because it is the only relevant time scale in the problem, the formation time of gluons after the collision is of order $1/Q_s$ [5,7]. The nuclei are highly Lorentz contracted—the pressure gradients in the longitudinal direction after the collision are therefore enormous and the system expands outwards at nearly the speed of light. The initial space-time evolution of the produced classical fields is described by solutions of Yang-Mills equations with CGC initial conditions [4,8–10]. The produced gluons begin to scatter; the strength of their scattering is determined by an infrared Debye mass m_D which screens the range of their interactions. The occupation number f of produced gluons, initially of order of the inverse strong coupling, $f \sim 1/\alpha_s$, decreases with time. It was believed initially that $2 \to 2$ [11] and later $2 \to 3$ [12,13] scattering processes could thermalize the system. Parametrically, however, these scattering processes take a long time of order $\tau_{\text{therm.}} \sim \frac{1}{\alpha_s^{13/5}} \frac{1}{Q_s}$ in the "bottom up"

thermalization scenario [13]. Matter in this preequilibrium phase, where several time scales compete, has been termed a "glasma" to describe its transitory behavior from coherent color glass fields to thermalized quark gluon plasma [14].

It has been suggested for some time that instabilities, analogous to the Weibel instability [15] in plasma physics, may play an important role in thermalization of the glasma [16]. Recently, the specific mechanism in the "color glass/bottom up" scenario triggering the instability was identified [17] as arising from the change in sign of the Debye mass squared for anisotropic momentum distributions [18]. One can view this, in the configuration space of the relevant fields, as the development of specific modes for which the effective potential is unbound from below [19]. Detailed simulations in the hard-loop effective theory in $1 + 1$-dimensions [17,19,20] and in $3 + 1$-dimensions [21,22] have confirmed the existence of this non-Abelian Weibel instability. Particle-field simulations of the effects of the instability on thermalization have also been performed recently [23,24].

All these simulations consider the effect of instabilities in systems at rest. However, as discussed previously, the glasma expands into the vacuum at nearly the speed of light. Recently, we presented first results on $3 + 1$-D numerical simulations of Yang-Mills equations which demonstrated the existence of a non-Abelian Weibel instability in the expanding glasma [25]. Such an instability was not seen in previous numerical simulations of the glasma [8–10] which assumed strict boost invariance, and therefore, dynamics in $2 + 1$ dimensions. Remarkably, arbitrarily weak violations of boost invariance trigger the non-Abelian Weibel instability. Another striking feature of our simulations was that the unstable fields in the expanding glasma grow proportional to $\exp(\Gamma\sqrt{g^2\mu\tau})$ as opposed to the usual exponential form. The former functional form was predicted by the authors of Ref. [17]. They deduced it simply from the fact that the scale for the growth rate in the

---

[1]In the CGC framework, this scale is simply related, in leading order, to μ^2, the color charge squared per unit area: $Q_s^2 = g^4\mu^2 N_c \ln(g^2\mu/\Lambda)/2\pi$, where Λ is an infrared cutoff.

expanding system is set by the Debye mass which depends on the proper time $\tau (= \sqrt{t^2 - z^2})$ as $m_D \propto 1/\sqrt{\tau}$.

In this work, we present more details and expand on the results presented in Ref. [25]. In particular, we look at much larger transverse and longitudinal lattices and study the dependence of the growth rate on the volume and continuum limits. Further, we extend the studies of Ref. [25] to much larger violations of boost invariance than considered previously. While kinematic violations of boost invariance are small, dynamical small x quantum evolution effects contribute to much larger violations of boost invariance. We consider one particular realization of such violations of boost invariance. We are able to follow all the stages of the evolution: we determine the time scale when the $\exp(\Gamma \sqrt{g^2 \mu \tau})$ growth of unstable modes starts to dominate over the initial spectrum, the saturation of the growth of these modes and the subsequent generation of longitudinal pressure as the system evolves towards isotropy. The time scales we obtain for this last stage are much larger than natural time scales for heavy-ion collisions.

Recently, a field theory formalism was developed to compute multiplicities in field theories with strong time dependent sources j (with $j \sim 1/g$, where g is the QCD coupling). The prototype for such a theory is the CGC [26]. In this framework, the results of Refs. [8–10] can be understood as a leading order contribution to the inclusive multiplicities, while the computation performed here can be seen as an (approximate) means of computing a piece of the next-to-leading order multiplicities. Other contributions are not included in this computation. (We will elaborate on these remarks in section V B.) Alternately, the results of Ref. [26] can be formulated as a Boltzmann equation with a source term [27]—the full next-to-leading order contributions will provide significant contributions towards thermalization. Our computations here must therefore be viewed as an essential but not exclusive piece of a complete computation of the evolution of the glasma into the QGP.

This paper is organized as follows. In Sec. II, we discuss the formulation of the problem of nuclear collisions in the CGC framework. In particular, we discuss how violations of boost invariance are implemented. We discuss details of the lattice formulation of the problem in the following section. In Sec. IV, we discuss numerical results for the non-Abelian Weibel instability. In particular, we study how the Fourier modes of the longitudinal pressure grow as a function of proper time. We show explicitly the distribution of unstable longitudinal ($\mathbf{k} || \mathbf{k_z}$) modes and their evolution. We note a very interesting behavior for the hardest momentum mode that is still unstable, $\nu_{\max}$: while otherwise growing slowly, $\nu_{\max}$ increases dramatically when the maximum amplitude of an unstable mode reaches a certain critical value. A plausible interpretation of this effect is that when the amplitude of the longitudinal fluctuations— which roughly translates as the amplitude of the unstable

transverse magnetic field modes—become large enough, the Lorentz force on transverse ($\mathbf{k} || \mathbf{k_\perp}$) ''particle'' modes of the gluon fields is sufficient for them to acquire significant longitudinal momenta. Hence the rapid increase in $\nu_{\max}$. This effect is enhanced for large boost invariance violating ''seeds,'' which are discussed further in Sec. V. Because this ''Lorentz force effect'' is significant for large seeds, we notice a rise in the longitudinal pressure, albeit the effect becomes measurable only at late times. The increase in the longitudinal pressure is accompanied by a decrease in the transverse pressure; this supports our conjecture that hard transverse gluon modes display a significant change in their trajectories when the modes of the transverse magnetic fields are large enough. We observe a clear trend towards isotropy and quantify the change in the dependence of the energy density with proper time. Despite this trend, the time scales over which these effects occur are much too large to explain the early thermalization at RHIC. This may be because, as discussed previously, our numerical simulations may not include all the processes necessary for thermalization. In the final section, we summarize our results and discuss work in progress [28] on thermalization in the glasma.

II. NUCLEAR COLLISIONS IN THE COLOR GLASS CONDENSATE

We will provide here a brief review of nuclear collisions in the color glass condensate framework. A more detailed discussion can be found in Ref. [2]. We will first discuss the 2 + 1-dimensional boost invariant formulation of the problem before extending our discussion to the more general 3 + 1-D problem.

A. Gluon production from classical fields

In nuclear collisions at very high energies, the hard valence parton modes in each of the nuclei act as highly Lorentz contracted, static sources of color charge for the soft wee parton, Weizsäcker-Williams modes in the nuclei. By hard and soft, we mean large x or small x, where x is the longitudinal momentum fraction of partons in the colliding nuclei. Soft x modes can be understood as modes that are coherent across the longitudinal extent of the nucleus, or equivalently, $x \ll A^{-1/3}$. With increasing energy, the scale separating soft and hard modes shifts towards smaller values of x. How the sources are modified with this changing scale is quantified by a Wilsonian RG procedure—a discussion and relevant references can be found in Ref. [2]. In a nuclear collision, the hard sources are described by the current

$$J^{\mu,a} = \delta^{\mu+} \rho_1^a(x_\perp) \delta(x^-) + \delta^{\mu-} \rho_2^a(x_\perp) \delta(x^+), \quad (1)$$

where the color charge densities $\rho_{1,2}^a$ of the two nuclei are independent sources of color charge on the light cone. Note that $x^\pm = (t \pm z)/2$. The δ functions represent the fact that

Lorentz contraction has squeezed the nuclei to infinitesimally thin sheets. The absence of a longitudinal size scale ensures that the gauge fields generated by these currents will be boost invariant, namely, independent of the space-time rapidity $\eta = a\tanh\frac{z}{t}$. The gauge fields before the collision are obtained by solving the Yang-Mills equations $D_\mu F^{\mu\nu} = j^\nu$, with

$$D_\mu = \partial_\mu + ig[A_\mu, .],$$
$$F_{\mu\nu} = \partial_\mu A_\nu - \partial_\nu A_\mu + ig[A_\mu, A_\nu], \tag{2}$$

the gauge covariant derivative and field strength tensor, respectively, in the fundamental representation, and $[A_\mu, .]$ denotes a commutator.

Gluon distributions are simply related to the Fourier transform $A_\mu(k_\perp)$ of the solution of the Yang-Mills equations by $\langle A_\mu(k_\perp)A_\mu(k_\perp)\rangle_\rho$. The averaging over the classical charge distributions is defined by the expression

$$\langle O\rangle_\rho = \int d\rho_1 d\rho_2 O(\rho_1, \rho_2)$$
$$\times \exp\left(-\int d^2x_\perp \frac{\mathrm{Tr}[\rho_1^2(x_\perp) + \rho_2^2(x_\perp)]}{2\mu^2}\right), \tag{3}$$

and is performed independently for each nucleus with equal Gaussian weight μ^2. Here $\mu^2 \propto A^{1/3}$ fm^{-2} denotes the color charge squared per unit area in each of the (identical) nuclei with atomic number A. For very large nuclei, μ is much larger than the fundamental QCD scale, $\mu^2 >> \Lambda_{QCD}^2$—this asymptotic condition justifies our applying weak coupling techniques to the problem. Such a Gaussian weight is justified [3,29,30] in the limit of $A \gg 1$ and $\alpha_s Y \ll 1$, providing a window $\ln(A^{1/3}) < Y < A^{1/6}$ in rapidity[2] Y, which exists for large A. This window of applicability, for large nuclei, can be extended to larger values of Y by using the Balitsky-Kovchegov equation [31] to evolve the sources $\rho_{1,2}$ to higher rapidities. This small x renormalization group evolution of the source densities preserves the Gaussian structure of the sources—however, it is now nonlocal and $\mu^2 \to \mu^2(x_\perp - y_\perp)$. We do not expect this generalization to qualitatively modify the results discussed here. We will return to this discussion when we discuss violations of boost invariance.

Before the nuclei collide ($t < 0$), a solution of the equations of motion is [3]

$$A^\pm = 0; \tag{4}$$
$$A^i = \theta_\epsilon(x^-)\theta_\epsilon(-x^+)\alpha_1^i(x_\perp) + \theta_\epsilon(x^+)\theta_\epsilon(-x^-)\alpha_2^i(x_\perp),$$

where, here and in the following, the transverse coordinates x, y have been collectively labeled by the Latin index i. The ϵ subscripts on the θ-functions denote that they are smeared by an amount ϵ in the respective $x^\pm$ light cone

directions. We require that the functions $\alpha_m^i(x_\perp)$ ($m = 1, 2$ denote the labels of the colliding nuclei) satisfy $F^{ij} = 0$, namely, that they be pure gauge solutions of the equations of motion. The functions α_m^i satisfy

$$-D_i\alpha_{(m)}^i = \rho_{(m)}(\mathbf{x}_\perp). \tag{5}$$

This equation has an analytical solution given by [29,32]

$$\alpha_{(m)}^i = \frac{-i}{g}e^{i\Lambda_{(m)}}\partial^i e^{-i\Lambda_{(m)}}, \qquad \nabla_\perp^2 \Lambda_{(m)} = -g\rho_{(m)}. \tag{6}$$

To obtain this result one has to assume path ordering in $x^\pm$ respectively for nuclei 1 and 2; we assume that the limit $\epsilon \to 0$ is taken at the final step.

We now introduce the proper time $\tau = \sqrt{t^2 - z^2} = \sqrt{2x^+ x^-}$—the initial conditions for the evolution of the gauge field in the collision are formulated on the proper time surface $\tau = 0$. They are obtained [4] by generalizing the previous ansatz for the gauge field to

$$A^i(x^-, x^+, x^\perp) = \Theta_\epsilon(x^-)\Theta_\epsilon(-x^+)\alpha_1^i(x_\perp)$$
$$+ \Theta_\epsilon(-x^-)\Theta_\epsilon(x^+)\alpha_2^i(x_\perp)$$
$$+ \Theta_\epsilon(x^-)\Theta_\epsilon(x^+)\alpha_3^i(x^-, x^+, x^\perp) \tag{7}$$
$$A^\pm = \pm x^\pm \Theta_\epsilon(x^-)\Theta_\epsilon(x^+)\beta(x^-, x^+, x^\perp),$$

where we adopt the Fock-Schwinger gauge condition $A^\tau \equiv x^+ A^- + x^- A^+ = 0$. This gauge is an interpolation between the two light cone gauges $A^\pm$ on the $x^\pm = 0$ surfaces, respectively. The sole purpose of the ansatz for the gauge fields here is to obtain the unknown gauge fields α_3, β in the forward light cone from the known gauge fields $\alpha_{(1,2)}$ of the respective nuclei before the collision. This is achieved by invoking a physical "matching condition" which requires that the Yang-Mills equations $D_\mu F^{\mu\nu} = J^\nu$ be regular at $\tau = 0$. The δ-functions of the current in the Yang-Mills equations therefore have to cancel identical terms in spatial derivatives of the field strengths. Interestingly, it leads to the unique solution [4]

$$\alpha_3^i(x^+, x^-, x^\perp) = \alpha_1^i(x^\perp) + \alpha_2^i(x^\perp),$$
$$\beta(x^+, x^-, x^\perp) = -\tfrac{1}{2}ig[\alpha_{i,1}(x_\perp), \alpha_2^i(x_\perp)]. \tag{8}$$

Further, the only condition on the derivatives of the fields that would lead to regular solutions are $\partial_\tau\alpha|_{\tau=0}$, $\partial_\tau\alpha_\perp^i|_{\tau=0} = 0$. This completes the derivation of the initial conditions in the boost-invariant case.

Gyulassy and McLerran [33] argue that the equations of motion with the above boundary conditions remain unchanged even when the fields $\alpha_{1,2}^i$ before the collision are smeared out in rapidity to properly account for singular contact terms in the equations of motion. We concur and will discuss violations of boost invariance later.

---

[2]Here we refer to the momentum space rapidity $Y = \frac{1}{2} \times \ln(\frac{E+p_z}{E-p_z}) \equiv Y_{\mathrm{beam}} - \ln(\frac{1}{x})$.

B. Hamiltonian chromodynamics in τ, η coordinates

While the Yang-Mills equations discussed above can be solved perturbatively [4,33,34] in the limit $\alpha_s \mu \ll k_\perp$, it is unlikely that a simple analytical solution exists in general. The classical solutions have to be determined numerically for $\tau > 0$. The straightforward procedure would be to discretize the Yang-Mills equations. However, gauge invariance is best ensured by solving Hamilton's equations on the lattice. In practice therefore, we need to construct the lattice Hamiltonian and obtain the corresponding lattice equations of motion.

The gluonic part of the QCD action in general coordinates takes the form

$$S = -\frac{1}{2} \int d\tau d\eta dx_\perp \sqrt{-\det g_{\mu\nu}}$$
$$\times \mathrm{Tr}[F_{\mu\nu} g^{\mu\alpha} g^{\nu\beta} F_{\alpha\beta} + j_\mu g^{\mu\nu} A_\nu] \qquad (9)$$
$$= \int d\tau d\eta dx_\perp \mathcal{L},$$

where for convenience we choose to keep the gauge-covariant but not coordinate-covariant $F_{\mu\nu}$ defined by Eq. (2). For the purpose of solving the Yang-Mills equations for a heavy-ion collision on a lattice, we shall work in the light cone coordinates $\tau = \sqrt{2x^+ x^-}$ and $\eta = \frac{1}{2} \ln(\frac{x^+}{x^-})$. Our gauge condition $x^+ A^- + x^- A^+ = 0$ transforms to $A^\tau = 0$, and the Lagrangian density becomes

$$\mathcal{L} = \tau \mathrm{Tr}\left[\frac{F_{\tau\eta}^2}{\tau^2} + F_{\tau i}^2 - \frac{F_{\eta i}^2}{\tau^2} - \frac{F_{ij}^2}{2} + \frac{j_\eta A_\eta}{\tau^2}\right], \qquad (10)$$

due to the nontrivial metric $g_{\mu\nu} = \mathbf{diag}(1, -1, -1, -\tau^2)$. Note that the contribution of the hard valence current to $\mathcal{L}$ drops out in the boost-invariant case[3] and can be neglected as long as one only considers a small region around central space-time rapidities $\eta = 0$. The conjugate momenta are then

$$E_i = \frac{\partial \mathcal{L}}{\partial(\partial_\tau A_i)} = \tau \partial_\tau A_i, \qquad E_\eta = \frac{\partial \mathcal{L}}{\partial(\partial_\tau A_\eta)} = \frac{1}{\tau} \partial_\tau A_\eta$$
$$(11)$$

which we use to construct the Hamiltonian density

$$\mathcal{H} = E_i(\partial_\tau A_i) + E_\eta(\partial_\tau A_\eta) - \mathcal{L}$$
$$= \mathrm{Tr}\left[\frac{E_i^2}{\tau} + \frac{F_{\eta i}^2}{\tau} + \tau E_\eta^2 + \tau F_{xy}^2\right]. \qquad (12)$$

Using finally

$$\frac{\partial \mathcal{H}}{\partial E_\mu} = \partial_\tau A_\mu, \qquad \frac{\partial \mathcal{H}}{\partial A_\mu} = -\partial_\tau E_\mu, \qquad (13)$$

---

[3] As we shall see, the dependence on the source densities is contained in the initial conditions through the dependence of the gauge fields on the source densities.

one finds the equations of motion in the Hamiltonian formulation,

$$\partial_\tau A_i = \frac{E_i}{\tau}, \qquad \partial_\tau A_\eta = \tau E_\eta$$
$$\partial_\tau E_i = \tau D_j F_{ji} + \tau^{-1} D_\eta F_{\eta i} \qquad \partial_\tau E_\eta = \tau^{-1} D_j F_{j\eta}.$$
$$(14)$$

The Gauss law constraint is simply

$$D_i E_i + D_\eta E_\eta = 0. \qquad (15)$$

If the sources are strictly δ-function sources on the light cone, the Yang-Mills equations are independent of the space-time rapidity. One therefore has

$$A_i(x_\perp, \eta, \tau) \equiv A_i(x_\perp, \tau); \qquad A_\eta \equiv \Phi(x_\perp, \tau), \qquad (16)$$

which results in $F_{\eta i} = -D_i \Phi$. The Hamiltonian in Eq. (12) then reduces in the boost-invariant case to

$$\mathcal{H} = E_i(\partial_\tau A_i) + E_\eta(\partial_\tau A_\eta) - \mathcal{L}$$
$$= \mathrm{Tr}\left[\frac{E_i^2}{\tau} + \frac{(D_i \Phi)^2}{\tau} + \tau E_\eta^2 + \tau F_{xy}^2\right], \qquad (17)$$

which is the QCD Hamiltonian in $2 + 1$-dimensions coupled to an adjoint scalar field. Boost invariance clearly greatly simplifies the numerical simulations of these equations of motion.

The initial conditions for the gauge fields in the boost-invariant case from Eq. (8) become

$$A^i(x_\perp) = \alpha_{(1)}^i(x_\perp) + \alpha_{(2)}^i(x_\perp), \qquad A_\eta(x_\perp) = 0,$$
$$E_i(x_\perp) = 0, \qquad E_\eta(x_\perp) = ig[\alpha_{(1)}^i, \alpha_{(2)}^i]. \qquad (18)$$

The magnetic fields being defined as $B_k = \epsilon_{k\mu\nu} F^{\mu\nu}$, these initial conditions suggest that $B_\eta \neq 0$ and $B_i = 0$. Note that the latter condition follows from the constraint on the derivatives of the gauge field that ensure regular solutions at $\tau = 0$. Thus one has $E_\eta, B_\eta \neq 0$ and large, as well as E_i, $B_i = 0$. This is in sharp contrast to the electric and magnetic fields of the nuclei before the collision—they are purely transverse. Some of the consequences of these initial conditions were discussed previously by Kharzeev, Krasnitz and Venugopalan [35]; their importance was emphasized recently by Lappi and McLerran [14].

C. Violations of boost invariance

In heavy-ion collisions, one clearly does not have exact boost invariance. Besides simple geometric effects (a heavy nucleus can never be Lorentz contracted into an infinitely thin sheet), one also has to take into account quantum fluctuations at high energies. These lead to violations of boost invariance that are of order unity over rapidity scales $Y \sim \alpha_s^{-1}$. Consequently, a more realistic model of a heavy-ion collision will have color sources that have a finite width in $x^\pm$ instead of the idealized δ

functions of Eq. (1). Nevertheless, the nuclei are highly localized on the light cone, and the same matching conditions required for regular solutions in the forward light cone apply.

We will assume here that the initial conditions in Eq. (8) can be extended to the boost noninvariant case. Ignoring details of exact matching of the Yang-Mills equations on the light cone, the qualitative difference with respect to idealized boost-invariant case are rapidity fluctuations due to violations of boost invariance. In what follows, we will study two models of initial conditions containing rapidity fluctuations.[4] We construct these by modifying the boost-invariant initial conditions in Eq. (18) to

$$
\begin{aligned}
E_i(x_\perp, \eta) &= \delta E_i(x_\perp, \eta), \\
E_\eta(x_\perp, \eta) &= ig[\alpha^i_{(1)}, \alpha^i_{(2)}] + \delta E_\eta(x_\perp, \eta)
\end{aligned}
\tag{19}
$$

while keeping A_i, A_η unchanged. The rapidity dependent perturbations δE_i, δE_η are in principle arbitrary, except for the requirement that they satisfy the previously mentioned Gauss law. For these initial conditions, it takes the form

$$
D_i \delta E_i + D_\eta E_\eta = 0. \tag{20}
$$

We construct these perturbations as follows:

(i) we first generate random configurations $\delta \bar{E}_i(x_\perp)$ with $\langle \delta \bar{E}_i(x_\perp) \delta \bar{E}_j(y_\perp) \rangle = \delta_{ij} \delta(x_\perp - y_\perp)$.

(ii) Next, for our first model of rapidity perturbations, we generate a Gaussian random function $F(\eta)$ with amplitude Δ

$$
\langle F(\eta) F(\eta') \rangle = \Delta^2 \delta(\eta - \eta'). \tag{21}
$$

For the second model, which we shall discuss further in Sec. V, we generate the Gaussian random function but then remove the high-frequency components of $F(\eta)$ by applying a "band-filter" with strength b:

$$
\begin{aligned}
F(\eta) \rightarrow F(\eta) = \int \frac{d\nu}{2\pi} \exp(-i\nu\eta) \exp(-|\nu|b) \\
\times \int d\eta \exp(i\eta\nu) F(\eta).
\end{aligned}
\tag{22}
$$

The white noise Gaussian fluctuations of the previous model ensure that the amplitudes of all modes are of the same size. The high momentum modes dominate bulk observables such as the pressure. The instability we will discuss shortly is sensitive to the infrared modes but its effects are obscured by the higher momentum modes. This is particularly acute for large violations of boost invariance. Damping

the high frequency modes of the white noise spectrum will therefore allow us to also study larger values of Δ, or "large seeds" that violate boost invariance.

(iii) For both models, once $F(\eta)$ is generated, we then obtain

$$
\begin{aligned}
\delta E_i(x_i, \eta) &= \partial_\eta F(\eta) \delta \bar{E}_i(x_\perp), \\
E_\eta(x_i, \eta) &= -F(\eta) D_i \delta \bar{E}_i(x_\perp).
\end{aligned}
\tag{23}
$$

This construction explicitly satisfies Gauss' law.

We note that in order to implement rapidity fluctuations in the above manner, one has to have $\tau > 0$. This is a consequence of the chosen coordinates and does not have a physical origin. We will therefore will use these initial conditions at $\tau = \tau_{\text{init}}$ with $0 < \tau_{\text{init}} \ll Q_s^{-1}$ and show our results are fairly independent on the specific choice of τ_{init}.

III. LATTICE SIMULATIONS

The Hamiltonian formulation in the last section is very convenient since it allows for a straightforward discretization that can be used to solve the Yang-Mills equations on a space-time lattice in (τ, x, y, η). We follow previous discussions of lattice equations of motion and initial conditions [8,9]. For the reader's convenience, these are reproduced in Appendix A. We work on a lattice that has periodic boundary conditions in the transverse plane as well as in space-time rapidity. This is justified as long as one is restricted to small rapidity volumes $|\eta| \ll 1$. The lattice parameters (all of which are dimensionless) are

(i) $N_\perp$, the number of lattice sites in the transverse direction,

(ii) N_η, the number of lattice sites in the longitudinal direction,

(iii) $g^2 \mu a_\perp$, the lattice spacing in the transverse direction,

(iv) a_η, the lattice spacing in the longitudinal direction,

(v) $\tau_{\text{init}}/a_\perp$, the proper time at which the 3-dimensional simulations are begun,

(vi) $\delta\tau$, the time stepping size,

(vii) Δ, the initial size of rapidity fluctuations,

(viii) b, the strength of the "band filter" for the large seed case [see Eq. (22)].

Of these, only the combinations $g^2 \mu a_\perp N_\perp \equiv g^2 \mu L$ and $a_\eta N_\eta \equiv L_\eta$ have a transparent physical meaning.[5] Given the energy of the collision and the size of the colliding nuclei, one can estimate $g^2 \mu$ [8,9,33]; since we have periodic boundary conditions, $L^2 = \pi R^2$. For RHIC collisions of gold nuclei, one has $g^2 \mu L \approx 120$; collisions of

---

[4]These models of violations of boost invariance are only weakly motivated at present. The only condition imposed is that these satisfy Gauss' law. A more complete theory should specify, from first principles, the initial conditions in the boost noninvariant case.

[5]The initial size of the rapidity fluctuations Δ and the band filter parameter b will presumably be further specified in a complete theory. For our present purposes, they will be treated as arbitrary parameters, and results presented for a large range in their values.

lead nuclei at LHC energies will be a factor of 2 larger. Also, L_η is the physical size of the region in η being studied. For the purposes of this study, we will consider $L_\eta = 1.6$ units of rapidity in most cases. The continuum limit is approached by keeping $g^2\mu L$ and L_η fixed while sending $\delta\tau \to 0$, $g^2\mu a_\perp \to 0$, $a_\eta \to 0$. For the 3-dimensional simulations, we still have to choose a value for τ_{init}, which should be such that for $\Delta = 0$ we stay very close to the result from the 2-dimensional simulations (for all of which $\tau_{\text{init}} = 0$). Thus, we set

$$\tau_{\text{init}} = 0.05 a_\perp, \qquad (24)$$

and later check how strongly the results obtained depend on this choice.

IV. THE WEIBEL INSTABILITY

The primary observables in simulations of classical Yang-Mills dynamics are the components of the energy-momentum tensor [9],

$$T^{\mu\nu} = -g^{\mu\alpha}g^{\nu\beta}g^{\gamma\delta}F_{\alpha\gamma}F_{\beta\delta} + \tfrac{1}{4}g^{\mu\nu}g^{\alpha\gamma}g^{\beta\delta}F_{\alpha\beta}F_{\gamma\delta} \qquad (25)$$

In particular,

$$T^{xx} + T^{yy} = 2\,\text{Tr}[F_{xy}^2 + E_\eta^2] \qquad (26)$$

$$\tau^2 T^{\eta\eta} = \tau^{-2}\,\text{Tr}[F_{\eta i}^2 + E_i^2] - \text{Tr}[F_{xy}^2 + E_\eta^2]. \qquad (27)$$

Furthermore, the relation $\mathcal{H} = \tau T^{\tau\tau} \equiv \tau(T^{xx} + T^{yy} + \tau^2 T^{\eta\eta})$ [cf. Eq. (12)] shows how the physical energy density $T^{\tau\tau}$ is related to the Hamiltonian density. Similarly, we introduce

$$\tau P_\perp = \frac{\tau}{2}(T^{xx} + T^{yy}), \qquad \tau P_L = \tau^3 T^{\eta\eta}, \qquad (28)$$

which correspond to τ times the mean transverse and longitudinal pressure, respectively.

When studying the time evolution of rapidity fluctuations, it is useful to introduce Fourier transforms of observables with respect to the rapidity. For example,

$$\tilde{P}_L(\tau, \nu, k_\perp = 0) = \int d\eta \exp(i\eta\nu)\langle P_L(\tau, x_\perp, \eta)\rangle_\perp, \qquad (29)$$

where $\langle\rangle_\perp$ denotes averaging over the transverse coordinates (x, y). Apart from $\nu = 0$, this quantity would be strictly zero in the boost-invariant ($\Delta = 0$) case, while for nonvanishing Δ and ν, $\tilde{P}_L(\nu)$ has a maximum amplitude for one specific momentum ν. Using a very small but finite value of Δ, this maximum amplitude is very much smaller than the corresponding amplitude of a typical

transverse momentum mode. The system is very anisotropic in momentum space and consequently prone to develop a Weibel-type plasma instability [15], as was shown previously in [25,36].

In order to illustrate some features of this instability, it is convenient to excite very low frequency rapidity modes. Thus, contrary to our earlier requirement, we have to use very large ($\Delta\eta \simeq 100$) rapidity volumes; note that we only use this for illustrative purposes and shall later consider much smaller volumes.

In Fig. 1 we show the ensemble-averaged $\tau\tilde{P}_L(\nu)$ for four different simulation times. The earliest time ($g^2\mu\tau \simeq 22$) shows the configuration before the instability sets in. Starting to overcome the effect of expansion at times $g^2\mu\tau \simeq 28$, the instability makes the amplitude of the soft modes grow like $\sim \exp(\sqrt{\tau})$ (see [25], but also [37] for a more detailed analysis). At times $g^2\mu\tau \simeq 72$ the amplitudes of the softest modes clearly differs from the starting configuration. The two later snapshots (for times $g^2\mu\tau \simeq 156$ and $g^2\mu\tau \simeq 288$) indicate that the growth rate of the unstable modes closely resembles the analytic prediction from hard-loop calculations [17,18]. Figure 1 also shows that the unstable mode with the highest mode number ν (which, in the following we will refer to as ν_{max}) moves to higher ν as a function of time. We will investigate the very interesting and suggestive behavior of ν_{max} more closely in the next section.

The unstable mode with the biggest growth rate (the cusp of the "bumps" in Fig. 1) also seems to move upwards in ν as a function of τ, but more slowly. We use this to define the average growth rate Γ^{av} by simply tracking the time evolution of the maximum amplitude of $\tau\tilde{P}_L(\nu)$ and fitting it with the functional form

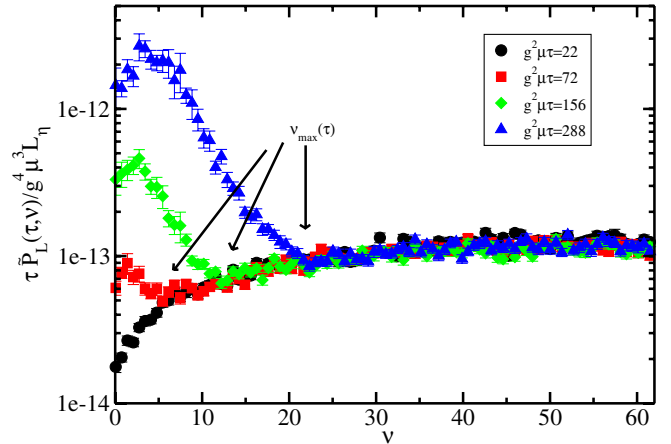FIG. 1 (color online). $\tau\tilde{P}_L(\tau, \nu)$ as a function of momentum ν, averaged over 160 initial conditions on a 16×2048 lattice with $g^2\mu L = 22.6$ and $L_\eta = 102.4$, $\Delta \simeq 10^{-11}$. Four different simulation times show how the softest modes start growing with a distribution reminiscent of results from hard-loop calculations [18]. Also indicated are the respective values of ν_{max} for three values of $g^2\mu\tau$ (see text for details).

$$c_0 + c_1 \exp(\Gamma^{av}_{fit} \sqrt{g^2 \mu \tau}). \qquad (30)$$

The label "average" refers to the fact that we do not fit the growth rate of a individual gauge mode but rather a convolution of modes contributing to every single ν of $\tau \tilde{P}_L(\nu)$. However, this method has the benefit of being a gauge-invariant measurement, while tracking the growth of individual gauge modes necessarily involves gauge-fixing procedures which we will address in the near future [28].

A. Results for the growth rate

Since the components of the energy-momentum tensor are gauge invariant, the fast rise of the soft longitudinal momentum occupation numbers cannot be a gauge artifact. Instead, in principle, this fast rise could be due to a lattice artifact rather than a physical instability. To convince the reader that this is not the case, we therefore present results in this section for the fitted average growth rates obtained for various values of the lattice parameters. The results are shown in Appendix B and indicate that the fitted average growth rate is close to $\Gamma^{av}_{fit} \simeq 0.5$, independent of our choices for a_η, $g^2 \mu a_\perp$, L_η, τ_{init}, Δ and having a weak dependence on $g^2 \mu L$. Our results suggest, unequivocally, that the instability present in the glasma is genuine and no lattice artifact.

B. Time evolution of ν_{max}

Physically, as suggested by Fig. 1, ν_{max} denotes the largest mode number that is sensitive to the instability. The technical method we use to determine ν_{max}, at a given τ, is to fit a high order polynomial to the momentum spectrum $\tau \tilde{P}_L(\tau, \nu)$ and find its section with a predefined "baseline" (a constant in ν and τ). Varying the baseline by a factor of $\sqrt{e} \simeq 1.65$ provides us with a rough estimate of

the error of our method. The time evolution of ν_{max} is plotted in Fig. 2 for different lattices.

From this figure, one observes an underlying trend indicating a linear increase of ν_{max} with approximately $\nu_{max} \simeq 0.06 g^2 \mu \tau$. For sufficiently small violations of boost invariance, this seems to be fairly independent of the transverse or longitudinal lattice spacing we have tested.

Presumably, this can be understood as follows: an unstable mode with wavelength Δz will correspond approximately to a wavelength $\Delta \eta$ as $\Delta \eta \simeq a \tanh \frac{\Delta z}{t}$. At late times (or central rapidities), we have $t \sim \tau \gg \Delta z$ and accordingly

$$\nu \sim \frac{\tau}{\Delta z}, \qquad (31)$$

where $\nu \sim (\Delta \eta)^{-1}$. In other words, the wavelength $\Delta \eta$ of the unstable mode would decrease (and ν increase) linearly as a function of τ for fixed Δz. This is precisely what is seen in Fig. 2. Turning the argument around, Fig. 2 provides us with a measure of the unstable mode wavelength Δz for large anisotropies, which cannot be calculated within a hard-loop framework.

For much larger violations of boost invariance—or sufficiently late times—one observes that ν_{max} deviates strongly from this "linear law." In Fig. 2 we show that this deviation seems to occur when the maximum amplitude of $\tau \tilde{P}_L(\tau, \nu)$ reaches a critical size, independent of other simulation parameters. This critical value is denoted by a dashed horizontal line and has the magnitude 3×10^{-5} in the dimensionless units plotted there. A possible explanation for this behavior is that the critical size of the longitudinal fluctuations [corresponding to transverse magnetic field modes with small $k_\perp$—see Eq. (27),(29)] is sufficient to bend particle (hard gauge mode) trajectories out of the
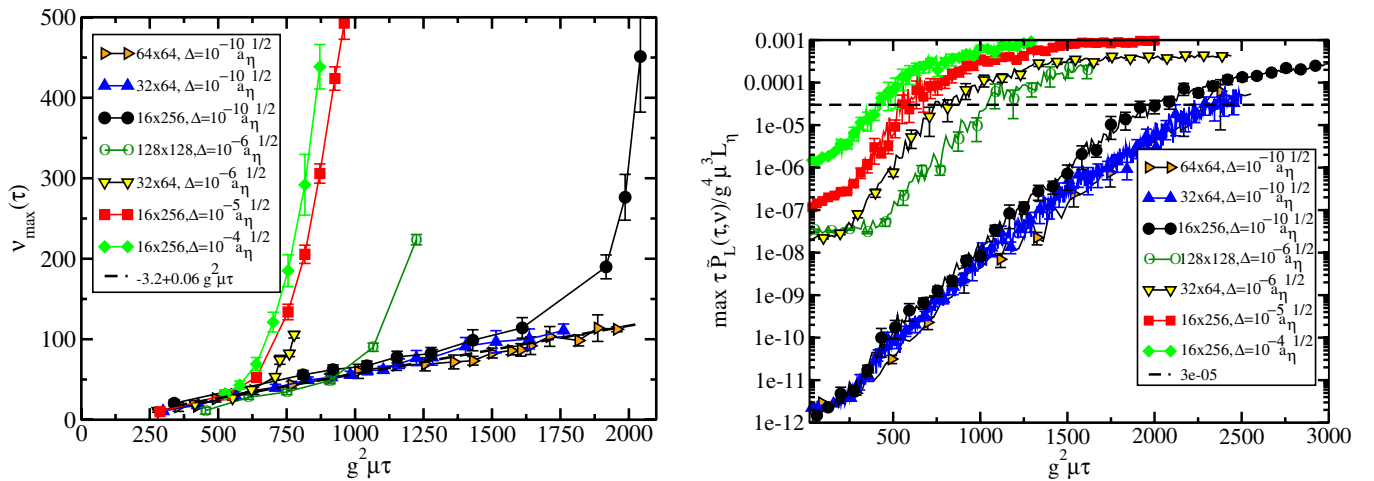

FIG. 2 (color online). Left: Time evolution of ν_{max}, on a lattices with $g^2 \mu L = 22.7$, $L_\eta = 1.6$ and various violations of boost invariance Δ. The dashed line represents the linear scaling behavior. Right: Time evolution of the maximum amplitude $\tau \tilde{P}_L(\tau, \nu)$; when this amplitude reaches a certain size (denoted by the dashed horizontal line), ν_{max} starts to grow fast.

transverse plane into the longitudinal direction. This is essentially what happens in electromagnetic plasmas. Note however that in electromagnetic plasmas, the particle modes are the charged fermions, while here the particle modes are hard ultraviolet transverse modes of the field itself.

In the next section, we will present results that indeed show that the transverse dynamics is visibly affected once the longitudinal fluctuations have reached a critical size. However, at the present, we cannot exclude the possibility that the rapid rise of $\nu_{\max}$ is due to a non-Abelian turbulent cascade as described in [38] or the phenomenon described in [24]. Clarifying this issue will require a detailed analysis of the time dependence of hard and soft modes [28].

V. LARGE SEEDS

In this section we focus on the (more realistic) model that involves large and predominantly soft momentum rapidity fluctuations. The only difference with respect to results from the previous section is the use of Eq. (22), where—unless otherwise stated—we used the value $b = 0.5$.

In Fig. 3, we plot the time evolution of the maximum amplitude of the ensemble averaged $\tau \tilde{P}_L(\tau, \nu)$, for lattices with different a_η. Early times in this figure ($g^2 \mu \tau < 200$) correspond to the stage when the Weibel instability is operative. Interestingly, all our simulations then show a saturation of the growth at approximately the same amplitude. This suggests that what one is seeing is similar to the phenomenon of "non-Abelian saturation," found in the context of simulations of plasma instabilities within the hard-loop framework [21,22]. However, while this result is robust for very large longitudinal lattices, further studies

involving much larger transverse lattices are required to conclusively establish this result.

A. Creation of longitudinal pressure

While for the small seed case the longitudinal fluctuations always carried only a tiny fraction of the total system energy the situation is different for the large seed case. In the simulations reported here, the initial energy contained in the longitudinal fluctuations is about 1% of the total system energy. In this subsection, we study the behavior of the time evolution of the average $P_L(\eta)$. This value is consistent with zero in simulations that do not allow for longitudinal dynamics. In Fig. 4 we plot P_L as a function of τ for different lattice spacings a_η. As can be seen, for large a_η (meaning low lattice UV cutoff), the longitudinal pressure is consistent with zero while it is clearly nonvanishing when the lattice UV cutoff is raised. However, there seems to be a limit to this rise as there is no notable difference between the simulations for the three smallest values of the lattice spacing. This is suggestive that the rise in the longitudinal pressure is physical, though again, further studies on even larger transverse lattices are needed to strengthen this claim.

B. Towards isotropy

In Fig. 5, we investigate the time evolution of the transverse pressure as well as the energy density for (i) a simulation with a low UV cutoff (16×32 lattice) and (ii) a simulation with a high UV cutoff (16×2048 lattice). We observe that the rise in the mean longitudinal pressure accompanies a drop both in the mean transverse pressure and energy density, thus bringing the system closer to an isotropic state. The energy density depends on the proper
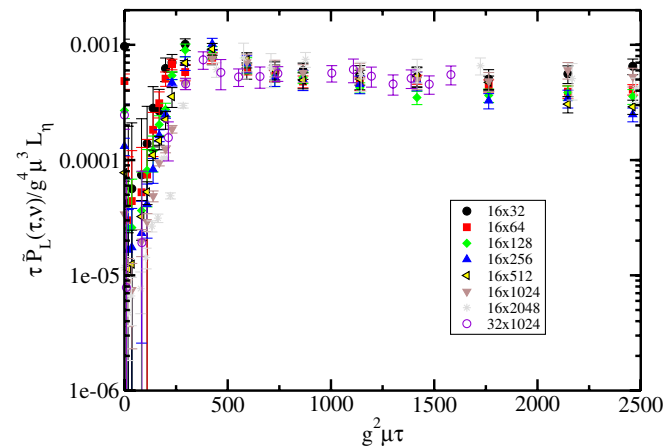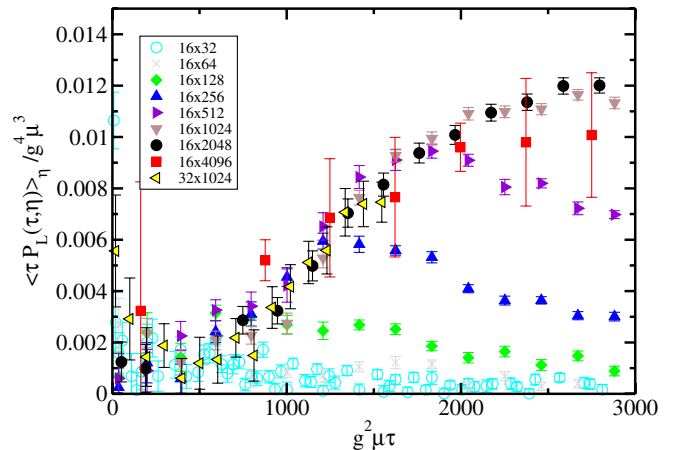

FIG. 3 (color online). Time evolution of the (ensemble-averaged) maximum amplitude of $\tau \tilde{P}_L(\tau, \nu)$, for $g^2 \mu L = 22.6$, $L_\eta = 1.6$, $N_\perp = 16, 32$, $\Delta = 0.1 a_\eta^{1/2}$ and N_η ranging from 32 to 2048. Larger lattices correspond to smaller Δ. This explains why the early-time behavior is not universal for the simulations shown here.

FIG. 4 (color online). Time evolution of the ensemble and volume averaged longitudinal pressure P_L, for lattices with $g^2 \mu L = 22.6$, $L_\eta = 1.6$, $N_\perp = 16, 32$, $\Delta = 0.1 a_\eta^{1/2}$ and N_η ranging from 32 to 2048. A reduced statistical ensemble of only 2 runs for $N_\eta = 4096$ is consistent with $N_\eta = 1024$, 2048 results within error bars.
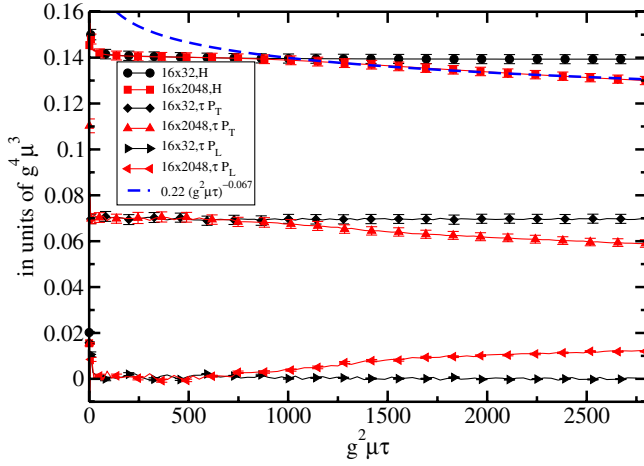
FIG. 5 (color online). Volume and ensemble averaged Hamiltonian density $\langle H(\tau, \eta)\rangle_\eta$ (corresponding to τ times energy density) and transverse and longitudinal pressure $\tau\langle P_T(\tau, \eta)\rangle_\eta$, $\tau\langle P_L(\tau, \eta)\rangle_\eta$, for simulations with small (16×32 lattice) and large (16×2048 lattice) longitudinal UV cutoff; quantities are multiplied by τ to facilitate comparison. The system evolves towards a more isotropic state if the UV cutoff is sufficiently large. A fit shows that the energy density behaves as $\varepsilon \sim \tau^{-1.067}$ at late times. All curves calculated on lattices with $g^2\mu L = 22.6$, $L_\eta = 1.6$ and $\Delta = 0.1a_\eta^{1/2}$.

time as $\varepsilon \sim \frac{1}{\tau^{1.067}}$, which is distinct from $\varepsilon \sim \frac{1}{\tau^{4/3}}$ for an isotropic system. Despite this clear trend, no full isotropization was achieved in these simulations on the time scales under investigation.

Why is this so? We digress here to emphasize, as discussed previously, that while simulations of the classical equations of motion capture important aspects of the early time dynamics, they miss others. What contributions are included in the numerical simulations here, and what contributions are not, can be understood in a systematic formalism developed recently to treat the real time nonequilibrium dynamics of fields in the presence of strong ($j \sim \frac{1}{g}$) time dependent sources [26]. The power counting in these theories, as discussed in Ref. [26], is entirely in powers of $g^2\hbar$. In this power counting, the 2 + 1-dimensional boost invariant classical solution provides the leading contribution of order $1/g^2\hbar$ to the average particle multiplicity—but includes all orders in the sources ($gj \sim O(1)$). This leading order result was computed numerically by Krasnitz, Nara and Venugopalan [8,9] and by Lappi [10]. At next-to-leading order (NLO), which is of order $(g^2\hbar)^0$, there are two contributions to the average multiplicity: (I) from the small fluctuations propagator, and (II) from the product of the classical field at lowest order and the classical field at one loop order. NLO contributions of type I are obtained by solving partial differential equations (with retarded boundary conditions) for small fluctuations on top of the classical background field. The procedure followed here is very similar in spirit: we add

fluctuations δE_i and δE_η on top of the boost invariant classical solutions and study their evolution in time. Whether these are identical to the NLO contributions is a topic under active investigation and beyond the scope of this paper (but which will be addressed further in a forthcoming work [27]). However, it is clear that contributions similar to the type II NLO contributions are not included in our simulation.

It has been argued [39] that the early time classical dynamics can be smoothly matched on to a Boltzmann equation. Interestingly, the previously mentioned NLO contributions may be clearly identified in the Boltzmann equation correspondence of Ref. [39]—such a study would shed further light on whether the additional processes not included in the study here may play a role in speeding up thermalization.

In any case, since the present study is based on classical field dynamics only, reaching true thermal equilibrium is beyond the capabilities of our simulation since description of the late stages of the evolution necessarily require the inclusion of quantum effects. Nevertheless, we believe that our study is at least qualitatively valid until the onset of the equilibration process, e.g. the point where the energy density has departed from the free-streaming behavior $\epsilon \sim \tau^{-1}$. As argued above, adding quantum effects through the full inclusion of the NLO contributions may be used to extend the domain of applicability of such simulations.

We return to our discussion to note, however, that increasing the seed parameter Δ further pushes the trend toward isotropization to earlier times. In Fig. 6, we plot the time evolution P_T/P_L as a measure of the system anisotropy for three values of Δ. One observes that larger values of Δ accompany an earlier set-in of the isotropization process. It should also be noted that increasing Δ further has the effect of strongly increasing the total system energy at early times.
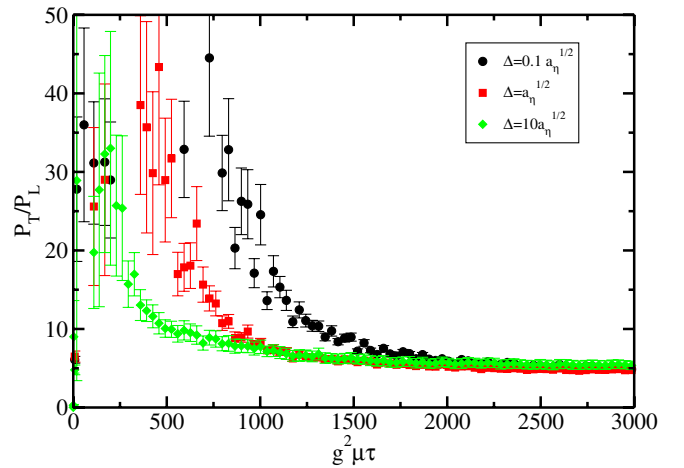

FIG. 6 (color online). The mean system anisotropy as measured by P_T/P_L for various values of Δ. Note that the late-times values could be subject to finite lattice spacing artifacts.

Similar to increasing Δ, one can also decrease the value of b (where we recall that this is the parameter that controls the initial exponential falloff of the momentum spectrum). Decreasing b by a factor of 5 results in a system anisotropy that is similar to the values for $\Delta = 10a_\eta^{1/2}$ in Fig. 6.

We conclude here that a first principles analytic computation of Δ and b would be extremely useful because quantitative results for the system isotropization time scale appear to depend on them strongly.

VI. CONCLUSIONS AND OUTLOOK

We discussed here detailed results from numerical simulations of $3 + 1$-D SU(2) Yang-Mills equations for an unstable glasma expanding into the vacuum after a high energy heavy-ion collision. This work greatly expands on our earlier paper [25] where first results for $3 + 1$-D numerical simulations were presented. Specifically, we explained in detail the set of initial conditions we are studying, providing details of our numerical simulations, and tested that our results were robust in the longitudinal and transverse continuum limits. A novel addition to our previous studies is a detailed study of large violations of boost invariance.

We established that for color glass condensate initial conditions, a Weibel instability is present in the system that appears as rapidly growing longitudinal fluctuations (starting in the far infrared) from times of $g^2\mu\tau \sim 30$ onwards. We performed detailed checks on the largest available lattices that the measured growth rate seems to be nearly independent of all our lattice parameters. We have demonstrated that the presence of the instability is very unlikely to be a lattice artifact.

We investigated the distribution of the unstable modes and found it to be strikingly similar to the analytic results from hard-loop calculations [17,18,40]. The time evolution of the maximum amplitude of these modes indicate a saturation of the growth at a certain size. This effect appears to be identical to the phenomenon of non-Abelian saturation described within the hard-loop framework [21,22]. Tracking the time evolution of the hardest unstable mode, ν_{max}, we deduced that the smallest unstable wavelength Δz is finite even for extreme anisotropies. This goes beyond results from hard-loop techniques.

We find further that when the longitudinal fluctuations reach a critical size, ν_{max} increases dramatically filling up the mode spectrum. Because this effect is simultaneously accompanied by a drop in the transverse pressure, we interpret this result as the effect of the Lorentz force exerted by modes of the transverse magnetic fields on the hard transverse gauge modes. These fields effectively bend the hard transverse gauge modes into the longitudinal direction. Note that the total amplitude of the transverse magnetic field does not increase significantly. Nevertheless, the ''bending'' can be accomplished since the

instability has populated predominantly modes with $k_\perp = 0$ and the corresponding transverse magnetic fields thus can act over long transverse distances.

Simulations on lattices with large longitudinal UV cutoff suggest that significant longitudinal pressure is built up in this process. This therefore shows a clear trend towards isotropization of the system. It is also reflected in the time evolution of the energy density. The energy density changes from the free streaming $\epsilon \sim \tau^{-1}$ behavior to $\epsilon \sim \tau^{-1.067}$. Our results are therefore proof in principle that a trend towards isotropization within a weak coupling framework is indeed possible, contrary to recent claims [41].

However, the time scales associated with isotropization in our simulations, are much too large in order to be of interest for phenomenology in heavy-ion collisions. This may be due to the fact, as discussed in Sec. V B, that we are only partly including next-to-leading order corrections in our framework [26]. While these contributions are formally NLO and may be presumed small, they properly treat number changing processes. In this regard, they may be considered leading order effects in driving the system towards equilibration. We should note further that our results strongly indicate that isotropization time scales are much shorter if longitudinal fluctuations are already large initially than if they have to be built up by the instability. A first principles calculation of the longitudinal gluon spectrum after a heavy-ion collision would thus probably be a key ingredient in understanding the process of equilibration.

APPENDIX A: LATTICE DISCRETIZATION

Introducing the lattice gauge links $U_i = \exp(iga_\perp A_i)$, $U_\eta = \exp(iga_\eta A_\eta)$, and making the fields dimensionless by scaling out the transverse lattice spacing $a_\perp$ and the coupling for convenience,

$$A_i \rightarrow \frac{A_i}{ga_\perp}, \qquad E_i \rightarrow \frac{E_i}{ga_\perp},$$

$$A_\eta \rightarrow \frac{A_\eta}{g}, \qquad E_\eta \rightarrow \frac{E_\eta}{ga_\perp^2} \tag{A1}$$

the discretized form of the Hamiltonian density equation (12) becomes the analog of the Kogut-Susskind Hamiltonian,

$$\mathcal{H}_L = \frac{1}{\tau g^2 a_\perp^3} \text{Tr}\left[E_i^2 + \tau^2 E_\eta^2 + \frac{2}{a_\eta^2}\sum_i (1 - \text{Re}U_{\eta,i}) + 2\tau^2 \sum_\square (1 - \text{Re}U_\square) \right], \tag{A2}$$

where we also scaled the lattice time $\tau \to \tau_L = \tau/a_\perp$; $U_\square = U_{i,j}$ with the standard plaquette $U_{\mu,\nu}(x) = U_\mu(x)U_\nu(x + \mu)U_\mu^\dagger(x + \nu)U_\nu^\dagger(x)$. The lattice equations of motion then become

$$E_i^a\left(\tau_L + \frac{\delta\tau_L}{2}, x\right) = E_i\left(\tau_L - \frac{\delta\tau_L}{2}, x\right) + 2i\delta\tau_L\tau_L \, \text{Tr}\left(\tau^a U_i(\tau_L, x) \sum_{|j|\neq i} S_{ij}^\dagger(\tau_L, x)\right) + 2i\frac{\delta\tau_L}{\tau_L a_\eta^2}\, \text{Tr}\left(\tau^a U_i(\tau_L, x)\sum_{|\eta|\neq i} S_{i\eta}^\dagger(\tau_L, x)\right)$$

$$E_\eta^a\left(\tau_L + \frac{\delta\tau_L}{2}, x\right) = E_\eta\left(\tau_L - \frac{\delta\tau_L}{2}, x\right) + 2i\frac{\delta\tau_L}{\tau_L a_\eta}\, \text{Tr}\left(\tau^a U_\eta(\tau_L, x) \sum_{|j|\neq\eta} S_{\eta j}^\dagger(\tau_L, x)\right)$$

$$U_i(\tau_L + \delta\tau_L, x) = \exp\left(i\delta\tau_L\tau_L^{-1}E_i\left(\tau_L + \frac{\delta\tau_L}{2}, x\right)\right)U_i(\tau_L, x)$$

$$U_\eta(\tau_L + \delta\tau_L, x) = \exp\left(i\delta\tau_L\tau_L a_\eta E_\eta\left(\tau_L + \frac{\delta\tau_L}{2}, x\right)\right)U_\eta(\tau_L, x) \tag{A3}$$

where

$$S_{\mu\nu}^\dagger(\tau_L, x) = U_\nu(\tau_L, x + \mu)U_\mu^\dagger(\tau_L, x + \nu)U_\mu^\dagger(\tau_L, x) \tag{A4}$$

is the gauge link staple. For SU(2), $E^i = E_a^i \tau^a$ with $\tau^a = \frac{1}{2}\sigma^a$ and σ^a the Pauli matrices and $\text{Tr}(\tau^a\tau^b) = \frac{1}{2}\delta^{ab}$. Note that the sum $\sum_{|j|\neq i}$ runs over both positive and negative directions, with $U_{-j}(\tau_L, x) = U_j^\dagger(x - j)$.

Numerical stability requires a very small $\delta\tau_L$ at the beginning of the simulation, but not at late times. Thus, we have found it convenient to use adaptive time steps, choosing

$$\delta\tau_L = \epsilon \frac{\tau}{\tau + T}, \tag{A5}$$

with $T \simeq 20$ and $\epsilon \simeq 0.025$ giving satisfactory performance for most simulations.

Initial conditions on the lattice

For SU(2), the initial conditions Eq. (18) lead to the following form of the gauge links [42]

$$U_i = (U_i^{(1)} + U_i^{(2)})(U_i^{(1)\dagger} + U_i^{(2)\dagger})^{-1} \tag{A6}$$

$$U_\eta = \mathbf{1}_2 \tag{A7}$$

$$U_i^{(1),(2)}(x) = V^{(1),(2)}(x)V^{(1),(2)}(x + i) \tag{A8}$$

$$V^{(1),(2)}(x) = \exp(i\Lambda_{1,2}(x)) \tag{A9}$$

$$\Delta_L\Lambda_{1,2}(x) = -\tilde{\rho}_{1,2}(x) \tag{A10}$$

$$\langle\tilde{\rho}_1^a(x)\tilde{\rho}_1^b(y)\rangle = g^4\mu^2 a_\perp^2\,\delta^{ab}\delta_{x,y}^2 \tag{A11}$$

$$\langle\tilde{\rho}_1^a(x)\tilde{\rho}_2^b(y)\rangle = 0, \tag{A12}$$

where x, y here denote site indices in the transverse plane and there is no summation over i on the left-hand side of the first equation. The last two equations should be understood such that the gauge configurations $\rho_{1,2}$ are drawn as Gaussian random numbers with weight $g^2\mu a_\perp$ while there should be no correlation between the different nuclei. Finally, Δ_L is the lattice Laplacian in the transverse plane,

$$\Delta_L\Lambda(x) = -2\Lambda(x) + \sum_i \Lambda(x + i) + \Lambda(x - i). \tag{A13}$$

The initial condition for the momenta for the boost-invariant case are

$$E_\eta^a = i\,\text{Tr}\tau^a \sum_i (U_i^{(2)}(x) + U_i^{(1)}(x)U_i^\dagger(x) - U_i^{(2)}(x - i)$$
$$- U_i^\dagger(x - i)U_i^{(1)}(x - i)) - \text{H.c.} \tag{A14}$$

together with $E_i^a(x) = 0$. The rapidity fluctuations are constructed as

$$\delta E_\eta^a = -F(x_\eta)D_i^{ab}\delta\bar{E}_i^b(x_\perp)$$
$$\delta E_i^a(x) = (F(x_\eta) - F(x_\eta - \eta))\delta\bar{E}_i^a(x_\perp)$$
$$\langle\delta\bar{E}_i^a(x_\perp)\delta\bar{E}_j^b(y_\perp)\rangle = \delta^{ab}\delta_{x_\perp,y_\perp}^2\delta_{ij} \tag{A15}$$
$$\langle F(x_\eta)F(x_\eta')\rangle = a_\eta^{-1}\Delta^2\delta_{x_\eta x_\eta'}.$$

For the case of large seeds, we modify $F(x_\eta)$ by creating its Fourier-transform w.r.t. rapidity,

$$\tilde{F}(\kappa) = \sum_{x_\eta} \exp(2\pi i\kappa x_\eta/N_\eta)F(x_\eta), \tag{A16}$$

removing the high-frequency modes and transforming back,

$$F(x_\eta) = \frac{1}{N_\eta} \sum_{\kappa \le N_\eta/2} \exp(-2\pi i \kappa x_\eta/N_\eta) \exp(-2\pi b|\kappa|/N_\eta/a_\eta)\tilde{F}(\kappa)$$

$$+ \frac{1}{N_\eta} \sum_{\kappa > N_\eta/2} \exp(-2\pi i \kappa x_\eta/N_\eta) \exp(2\pi b(|\kappa| - N_\eta)/N_\eta/a_\eta)\tilde{F}(\kappa).$$

APPENDIX B: MEASURED GROWTH RATES

We present here a collection of tables, I, II, III, IV, V, VI, and VII, with measured growth rates for various different lattice parameters.

TABLE I. Testing for the rapidity lattice spacing dependence on lattices with $g^2\mu L = 22.6$, $L_\eta = 1.6$ with $N_\perp = 16$ and $\Delta = 10^{-10}a_\eta^{1/2}$.

N_η	$\Gamma_{\text{fit}}^{\text{av}}$
32	0.50 ± 0.01
64	0.52 ± 0.02
128	0.52 ± 0.02
256	0.524 ± 0.016

TABLE II. Testing for the rapidity volume dependence on lattices with $g^2\mu L = 22.6$, $a_\eta = 0.05$ with $N_\perp = 16$ and $\Delta = 10^{-10}a_\eta^{1/2}$.

N_η	$\Gamma_{\text{fit}}^{\text{av}}$
32	0.5 ± 0.01
64	0.508 ± 0.012
128	0.488 ± 0.01
256	0.492 ± 0.016
512	0.543 ± 0.016

TABLE III. Testing for the transverse lattice spacing dependence on lattices with $g^2\mu L = 22.6$, $L_\eta = 1.6$ and $\Delta = 10^{-10}a_\eta^{1/2}$.

$N_\perp$	N_η	$\Gamma_{\text{fit}}^{\text{av}}$
16	32	0.50 ± 0.01
32	64	0.504 ± 0.01
64	64	0.488 ± 0.02

TABLE IV. Testing for the transverse volume dependence on lattices with $L_\eta = 1.6$ and $\Delta = 10^{-10}a_\eta^{1/2}$.

$N_\perp$	N_η	$g^2\mu L$	$\Gamma_{\text{fit}}^{\text{av}}$
16	32	22.6	0.50 ± 0.01
64	64	67.9	0.426 ± 0.01
128	64	90.5	0.45 ± 0.03
128	256	181	0.394 ± 0.04

TABLE V. Testing for the dependence on τ_{init} on lattices with $g^2\mu L = 22.7$, $L_\eta = 1.6$, $N_\perp = 32$, $N_\eta = 64$ and $\Delta = 10^{-10}a_\eta^{1/2}$.

$\tau_{\text{init}}/a_\perp$	$\Gamma_{\text{fit}}^{\text{av}}$
0.025	0.488 ± 0.014
0.05	0.504 ± 0.01
0.1	0.51 ± 0.01

TABLE VII. Testing for the dependence on the time step $\delta\tau$ lattices with $g^2\mu L = 22.7$, $L_\eta = 1.6$, $N_\perp = 32$, $N_\eta = 32$. Note that adaptive step sizes are used [see Eq. (A5)].

ϵ	$\Gamma_{\text{fit}}^{\text{av}}$
0.025	0.50 ± 0.01
0.0125	0.50 ± 0.01
0.006 25	0.51 ± 0.01

TABLE VI. Testing for the dependence on the initial seed amplitude Δ on lattices with $g^2\mu L = 22.7$, $L_\eta = 1.6$, $N_\perp = 32$, $N_\eta = 64$.

$-\log_{10}(\Delta a_\eta^{-1/2})$	$\Gamma_{\text{fit}}^{\text{av}}$
10	0.504 ± 0.01
6	0.514 ± 0.03
3	0.48 ± 0.05

[1] K. Adcox *et al.* (PHENIX collaboration), Nucl. Phys. **A757**, 184 (2005); J. Adams *et al.* (STAR collaboration), *ibid.* **A757**, 102 (2005); B. B. Back *et al.* (PHOBOS collaboration), *ibid.* **A757**, 28 (2005); I. Arsene *et al.* (BRAHMS collaboration), *ibid.* **A757**, 1 (2005).

[2] E. Iancu and R. Venugopalan, in *QGP3*, edited by R. C. Hwa *et al.* (World Scientific, Singapore, 2004).

[3] L. McLerran and R. Venugopalan, Phys. Rev. D **49**, 2233 (1994); **49**, 3352 (1994).**50**, 2225 (1994).

[4] A. Kovner, L. D. McLerran, and H. Weigert, Phys. Rev. D **52**, 3809 (1995); **52**, 6231 (1995).

[5] L. V. Gribov, E. M. Levin, and M. G. Ryskin, Phys. Rep. **100**, 1 (1983).

[6] A. H. Mueller and J-W. Qiu, Nucl. Phys. **B268**, 427 (1986).

[7] J. P. Blaizot and A. H. Mueller, Nucl. Phys. **B289**, 847 (1987).

[8] A. Krasnitz and R. Venugopalan, Phys. Rev. Lett. **84**, 4309 (2000); **86**, 1717 (2001).

[9] A. Krasnitz, Y. Nara, and R. Venugopalan, Phys. Rev. Lett. **87**, 192302 (2001); Nucl. Phys. **A717**, 268 (2003); **A727**, 427 (2003).

[10] T. Lappi, Phys. Rev. C **67**, 054903 (2003); hep-ph/0505095.

[11] A. H. Mueller, Nucl. Phys. **B572**, 227 (2000); Phys. Lett. B **475**, 220 (2000); J. Bjoraker and R. Venugopalan, Phys. Rev. C **63**, 024609 (2001).

[12] S. M. H. Wong, Phys. Rev. C **54**, 2588 (1996); Z. Xu and C. Greiner, Phys. Rev. C **71**, 064901 (2005).

[13] R. Baier, A. H. Mueller, D. Schiff, and D. T. Son, Phys. Lett. B **502**, 51 (2001).

[14] T. Lappi and L. McLerran, Nucl. Phys. **A772**, 200 (2006).

[15] E. S. Weibel, Phys. Rev. Lett. **2**, 83 (1959).

[16] S. Mrówczyński, Phys. Lett. B **214**, 587 (1988); **314**, 118 (1993); **393**, 26 (1997); J. Randrup and S. Mrówczyński, Phys. Rev. C **68**, 034909 (2003); S. Mrowczynski, Acta Phys. Pol. B **37**, 427 (2006).

[17] P. Arnold, J. Lenaghan, and G. D. Moore, J. High Energy Phys. 08 (2003) 002; P. Arnold, J. Lenaghan, G. D. Moore, and L. G. Yaffe, Phys. Rev. Lett. **94**, 072302 (2005).

[18] P. Romatschke and M. Strickland, Phys. Rev. D **68**, 036004 (2003); **70**, 116006 (2004).

[19] P. Arnold and J. Lenaghan, Phys. Rev. D **70**, 114007 (2004).

[20] A. Rebhan, P. Romatschke, and M. Strickland, Phys. Rev. Lett. **94**, 102303 (2005).

[21] P. Arnold, G. D. Moore, and L. G. Yaffe, Phys. Rev. D **72**, 054003 (2005).

[22] A. Rebhan, P. Romatschke, and M. Strickland, J. High Energy Phys. 09 (2005) 041.

[23] A. Dumitru and Y. Nara, Phys. Lett. B **621**, 89 (2005).

[24] A. Dumitru, Y. Nara, and M. Strickland, hep-ph/0604149.

[25] P. Romatschke and R. Venugopalan, Phys. Rev. Lett. **96**, 062302 (2006).

[26] F. Gelis and R. Venugopalan, hep-ph/0601209.

[27] F. Gelis, S. Jeon, and R. Venugopalan (unpublished).

[28] T. Lappi, P. Romatschke, and R. Venugopalan (unpublished).

[29] Yu. V. Kovchegov, Phys. Rev. D **54**, 5463 (1996); **55**, 5445 (1997).

[30] S. Jeon and R. Venugopalan, Phys. Rev. D **70**, 105012 (2004); **71**, 125003 (2005).

[31] I. Balitsky, Nucl. Phys. **B463**, 99 (1996); Yu. V. Kovchegov, Phys. Rev. D **61**, 074018 (2000).

[32] J. Jalilian-Marian, A. Kovner, L. D. McLerran, and H. Weigert, Phys. Rev. D **55**, 5414 (1997).

[33] M. Gyulassy and L. D. McLerran, Phys. Rev. C **56**, 2219 (1997).

[34] Y. V. Kovchegov and D. H. Rischke, Phys. Rev. C **56**, 1084 (1997).

[35] D. Kharzeev, A. Krasnitz, and R. Venugopalan, Phys. Lett. B **545**, 298 (2002).

[36] P. Romatschke and R. Venugopalan, hep-ph/0510292.

[37] P. Romatschke and A. Rebhan, hep-ph/0605064.

[38] P. Arnold and G. D. Moore, Phys. Rev. D **73**, 025013 (2006); **73**, 025006 (2006).

[39] A. H. Mueller and D. T. Son, Phys. Lett. B **582**, 279 (2004); S. Jeon, Phys. Rev. C **72**, 014907 (2005).

[40] B. Schenke, M. Strickland, C. Greiner, and M. H. Thoma, Phys. Rev. D **73**, 125004 (2006).

[41] Y. V. Kovchegov, Nucl. Phys. **A762**, 298 (2005).

[42] A. Krasnitz and R. Venugopalan, Nucl. Phys. **B557**, 237 (1999); R. Venugopalan, Acta Phys. Pol. B **30**, 3731 (1999).